Received: 21 March 2022 | Revised: 6 December 2023 | Accepted: 26 January 2024

DOI: 10.1002/app.55347

RESEARCH ARTICLE

Applied Polymer SCIENCE WILEY

Nanoflower hydroxyapatite's effect on the properties of resin-based dental composite

Kadir Sağır[1] | **Aysu Aydınoğlu**[2] | **Afife Binnaz Hazar Yoruç**[2]

[1]Department of Materials Science and Technology, Faculty of Science, Turkish-German University, Istanbul, Turkey

[2]Department of Metallurgical and Materials Engineering, Faculty of Chemical and Metallurgical Engineering, Yıldız Technical University, Istanbul, Turkey

Correspondence
Aysu Aydınoğlu, Department of Metallurgical and Materials Engineering, Faculty of Chemical and Metallurgical Engineering, Yıldız Technical University, Istanbul, Turkey.
Email: aysuaydn@yildiz.edu.tr

Funding information
Yildiz Technical University Scientific Research Projects Coordination Unit, Grant/Award Number: FBA-2020-3992

Abstract

To investigate the reinforcing effect of nanoflower-like hydroxyapatite (NFHA) in resin-based dental composites, we synthesized a novel NFHA using microwave irradiation (MW), hydrothermal treatment (HT), and sonochemical synthesis (SS). Silanized NFHA was then used as the reinforcing filler in dental resin composites. We characterized the structure and morphology of various HA nanostructures using x-ray diffraction, scanning electron microscope, and TEM. The mechanical performance of dental resin composites reinforced with silanized NFHA was measured using a universal testing machine. Spherical HA, synthesized through chemical precipitation (CP), served as the control group. One-way analysis of variance was employed for the statistical analysis of the acquired data. The results demonstrate that the nanoflower morphology significantly was improved mechanical and physical properties. After conducting trials, the NFHA synthesized using MW and HT showed a substantial enhancement in mechanical and physical properties compared to the other structures. Therefore, it can be concluded that NFHA can serve as a novel reinforcing HA filler, providing regenerative properties to resin composites with sufficient mechanical strength.

KEYWORDS

bioengineering, biomaterials, nanocrystals, nanoparticles, nanowires, resins

1 | INTRODUCTION

Dental composites, especially resin-based composites (RBCs), have markedly reshaped dentistry, presenting both aesthetic and functional alternatives to traditional amalgam fillings.[1] Composed of an organic polymer matrix mixed with inorganic filler particles, these composites blend durability with appealing aesthetics.[2,3] A standout feature of RBCs is their superior color matching to natural teeth, with some advanced formulas even offering translucency and fluorescence akin to natural teeth.[4–6] Despite these advantages, there are challenges. The curing process of RBCs can result in volumetric shrinkage, which may lead to postoperative sensitivity or a weaker seal between the tooth and the restoration.[7,8] In terms of durability, while advancements in fillers have strengthened RBCs, their lifespan might still be shorter than that of ceramic or gold restorations in high-stress mouth regions.[9] Recent research has emphasized optimizing the type and distribution of inorganic fillers in RBCs. By doing so, the aim is to extend the composite's lifespan and reduce the need for repairs, emphasizing the importance of fillers' shape, size, and type in enhancing the final product's mechanical strength.[10–12]

Silica is a popular filler in dental composites due to its improved mechanical strength and polishability.[13–16] However, its use raises several concerns. Potential release of nanosized silica particles may pose health risks, and while the risk in dental scenarios is deemed low, it is under continuous research.[17] Over time, silica fillers might discolor or stain more readily than other fillers, compromising aesthetic quality.[16,18–21] Improperly dispersed silica can create inconsistencies in composites, affecting their look and function.[22,23] Silica lacks radiopacity, posing challenges for dental x-ray evaluations.[22,24,25] Unlike hydroxyapatite (HA), silica doesn't promote tooth structure remineralization, a potential defense against secondary caries.[26–28] Conversely, HA, being a primary component of dentin and enamel,[29–31] makes an excellent dental resin composite filler.[31–33] It provides mechanical strength,[34–37] is radiopaque,[38,39] and can even promote remineralization,[40–42] sealing microgaps between composites and teeth,[43–45] which may reduce future cavity risks. Therefore, recent years have seen an explosion of interest in advanced materials such as nanostructures and nanocomposites across various fields, including dental science.[46] The potential for transforming dental composites using nanomaterials, particularly hydroxyapatite (HAP) nanoparticles synthesized through hydrothermal methods, is being widely recognized.[47] RBCs containing hydroxyapatite nanoparticles in various morphologies like nanospherical and nanorods have been investigated for dental applications.[47] While these materials offer improved mechanical properties compared to traditional fillers, they still have limitations that create a demand for alternative filler morphologies like nanoflower hydroxyapatite (NFHA). Spherical particles may not provide sufficient mechanical interlocking with the resin matrix, thereby offering suboptimal reinforcement.[48] Spherical shapes may not distribute stress efficiently, leading to localized points of failure in the composite material.[49] Nanospherical particles may settle over time, creating issues in filler distribution throughout the composite.[47] Nano-rods may offer strength along their length but may be weak along their diameter, leading to uneven mechanical properties.[50] Creating uniform nanorods can be more complicated and time-consuming compared to other shapes.[51] Nanorods have a higher tendency to aggregate, which may compromise the uniformity and mechanical properties of the composite.[52] As dental research moves away from using traditional spherical and irregular morphology filler phase components, towards nanofibers, nanowhiskers, and nanotube morphology components, it becomes crucial to understand the benefits of these novel structures.[46]

Novel research focusing on the synthesis of nanoflower-like serried hydroxyapatite (NFHA) has shown that adjustments in pH value and temperature effectively control the size and shape of the nanoflowers.[2,8,53–55] These advancements suggest that NFHA holds significant potential for improving dental composites, though more investigation is needed, particularly regarding the use of NFHA over nanospherical or nano-rod hydroxyapatite in RBCs. The unique morphology of NFHA can provide better mechanical interlocking with the resin matrix, which may lead to enhanced tensile and compressive strength (CS).[56] The structure of NFHA may distribute stress more uniformly, potentially reducing the likelihood of localized failures.[57] NFHA could provide better color stability and optical properties, making the composites more aesthetically pleasing.[58] NFHA, like other hydroxyapatite structures, can promote remineralization, but its unique structure may offer added advantages such as higher surface area for ion exchange.[59] With advancements in synthesis techniques, NFHA can be produced with controlled size and morphology, potentially offering a more versatile material for RBCs. In summary, while nanospherical and nanorods hydroxyapatite fillers in RBCs have their merits, their limitations in terms of mechanical strength, stress distribution, and other factors make NFHA a promising candidate for further research and application.

The method of NFHA synthesis also influences the properties of the resulting dental composites. Studies comparing microwave irradiation (MW) and hydrothermal synthesis (HS) with conventional and sonochemical synthesis (SS) found that NFHA produced by the former methods exhibited higher stability and mechanical strength in the resulting dental composites.[59] Thus, the choice of synthesis method can critically impact the performance of NFHA in dental applications. Regarding the synthesis of NFHA, methods such as the homogeneous hydrothermal precipitation method,[60] SS,[61] and MW[62] offer precise control over the size, shape, and other physicochemical properties of the NFHA. These synthesis methods thus enhance the functionality of NFHA in various applications, such as dental composites. In particular, the resulting NFHA exhibits improved compatibility with the resin matrix and strengthens the interfacial bond when treated with 3-methacryloxypropyltrimethoxysilane (γ-MPS), a silane coupling agent.[63] This highlights the potential of NFHA in addressing some of the traditional limitations of dental composites.

While there have been impressive advancements and encouraging results, there are still notable gaps in our understanding. In this research, our goal was to explore how NFHA could enhance the properties of dental resin composites. We developed and analyzed dental resin composites that included silanized NFHA as a reinforcing filler. For synthesizing NFHA, we employed three distinct techniques—hydrothermal precipitation, SS, and MW. We then modified these NFHA particles with

3-methacryloxypropyltrimethoxysilane (γ-MPS) to improve their compatibility with the resin matrix and fortify the bonding at the interface. For a side-by-side performance evaluation, our research also utilized dental resin composites containing silanized spherical shaped hydroxyapatite (IPHA). Moreover, we scrutinized the impact of different NFHA concentrations on the mechanical attributes of the dental resin composites. The incorporation of silanized NFHA into dental resin composites will significantly improve the mechanical properties of the material, including tensile strength, CS, and wear resistance, compared to composites containing traditional fillers like spherical shaped hydroxyapatite (IPHA). With this research, we aspire to make meaningful contributions to the evolution of durable and dependable dental restorative materials.

2 | MATERIALS AND METHODS

2.1 | Materials

Bisphenol A glycidyl methacrylate (Bis-GMA, 99%), tri(ethylene glycol) dimethacrylate (TEGDMA, 95%), camphorquinone (CQ, 97%), ethyl-4-dimethylaminobenzoate (4-EDMAB, 99%), diphenyl(2,4,6-trimethylbenzoyl) phosphineoxide (TPO, 98%), and 3-methacryloxypropyl trimethoxysilane (γ-MPS, 99%) were purchased from Sigma-Aldrich (Germany). Calcium nitrate tetrahydrate ($Ca(NO_3)_2.4H_2O$), diammonium hydrogen phosphate ($(NH_4)_2HPO_4$), and ethylenediaminetetraacetic acid (EDTA) used in the synthesis of dental composite filler phase were obtained from Merck, Darmstadt, Germany. Other sources of calcium and phosphorus, calcium chloride ($CaCl_2$) and disodium hydrogen phosphate dihydrate ($Na_2HPO_4.2H_2O$), were obtained from Acros Organics, Geel, Belgium. The chemicals were analytical grade and used without further purification.

2.2 | Methods

2.2.1 | Synthesis of hydroxyapatite

Hydroxyapatite (HA) with diverse morphologies was synthesized using various methods, including chemical precipitation (CP), MW (MW), HS, and SS. The Ca/P ratio for HA was set at 1.67 across all synthesis conditions. Among these methods, CP served as the conventional approach for producing spherical shaped HA structures (SHA), which acted as a control group based on our previous studies.[64] Briefly, 0.174 M $Ca(NO_3)_2.4H_2O$ and 0.1561 M $(NH_4)_2HPO_4$ were dissolved separately in simulated body fluid (SBF).[65] The phosphate solution was then added to the calcium solution at 37°C at a flow rate of 4 mL/min. The pH of the mixture was maintained at 7.4 using an ammonia solution prepared in SBF. A white precipitate formed, and the solution was stirred vigorously for 1 h. It was then left to age for 1 day at 37°C without stirring. The precipitated solution was filtered and repeatedly washed with ethanol and distilled water to remove impurities. The resulting filter cake was dried at 80°C for 24 h in an oven and then calcined at 900°C for 2 h using an electric furnace to improve crystallinity levels. The resulting powder was termed as spherical shaped HA synthesized with CP and was coded as SHA-CP.

MW, HS, and SS were used to produces nanoflower structured HA synthesis. EDTA was used as the nucleating agent in all methods.

The synthesis procedure of NFHA using microwave irradiation was modified from a method reported by Liu et al.[66] Briefly, 50 mL of 0.08 M $Ca(NO_3)_2.4H_2O$ and 50 mL of 0.08 M EDTA solutions were prepared SBF and mixed for a 15 min. Then 50 mL 0.048 M of $(NH_4)_2HPO_4$ phosphate solution is slowly added to the Ca-EDTA mixture. pH was adjusted to 12 using NaOH solution. After 1 h of vigorous mixing, the obtained mixture was put into microwave device (Multivawe Go, Anton Paar) of 700 W power at 110°C under ambient air for 30 min. After cooling to room temperature, the precipitate was filtered, washed with deionized water, and dried in oven under vacuum at 80°C for 2 h. Particles synthesized using microwave irridation was called as NFHA-MW.

Li's method[67] was modifed to obtain NFHA structures using HS. Briefly, 0.08 M $Ca(NO_3)_2.4H_2O$ and 0.08 M EDTA solutions were dissolved in 50 mL SBF solution by magnetic stirrer and 50 mL of 0.048 M $(NH_4)_2HPO_4$ solution is added dropwise for 3 min. After 1 h mixing resulted mixture was transferred into the hydrothermal reactor (304 stainless steel autoclave with 100 mL teflon reactor, custom made) and the reaction is carried out at 190°C for 5 h. Once the reaction completed, the precipitates were separated by centrifugation, washed with deionized water and ethanol in sequence, and then dried in vacuum oven at 80°C for 2 h. Particles synthesized using SS were called as NFHA-HS.

In a typical experiment of NFHA production with a SS we modified Chao's method.[68] Briefly, 50 mL of 0.5 M $Ca(NO_3)_2.4H_2O$ and 0.5 M EDTA mixture were added to 50 mL 0.3 M $(NH_4)_2HPO_4$ solution under magnetic stirring at room temperature. After vigorous stirring for 5 min, the final mixture was irradiated by continuous ultrasound (Sonopuls Serie 4000, BANDELIN) at a frequency of 28 kHz and with a power of 200 W for 90 min. The products were centrifuged, washed, and dried at 80°C for 24 h. Particles synthesized using SS were called as NFHA-SS.

2.2.2 | Preparation of nanosilica powders

Silica powders were obtained from silica solution Ludox HS-40 to be used as the filler phase of the dental composite. The detailed description of the SiO_2 preparation was given in our previous research.[69] Briefly, colloidal silica was decanted into a 250 mL glass flask and subsequently positioned in a rotary evaporator. The drying process was conducted at 40°C with a rotation speed of 80 rpm in the rotary evaporator. The resulting dried particulates were subjected to ball milling for 24 h. After milling, the particles were sieved using a 250-mesh (63 μm) screen to obtain silica fillers.

2.2.3 | Silanization of HA structures

Silanization was carried out in order to strengthen the adhesion bonds between the filler phase and the organic matrix and to direct the filler phase from the hydrophilic structure to the hydrophobic structure. Our previous method[69] has been modified for the silanization of silica, SHA-CP, NFHA-MW, NFHA-HS, and NFHA-SS. Briefly, 1 mL (10 wt%) 3-MPTS and 0.2 g propylamine was added to the 100 mL acetone: water (7:3) solution were stirred under nitrogen atmosphere in a closed system at room temperature for 15 min. It was subsequently subjected to heating at 65°C for a duration of 60 min. The mixture underwent drying via a rotary evaporator at 60°C to eliminate volatile substances and was subsequently heated at 95°C for 2 h. Finally, the resulting product was dried in a vacuum oven at 85°C for a total of 18 h.

2.2.4 | Preparation of resin-based dental composites

In order to prepare the experimental resin, BisGMA (1%–5%) was kept for 10 min at 40°C in the ultrasonic water bath and then HEMA (5–10 wt%), UDMA (5–10 wt%), and TEGDMA (1–5 wt%) were added. TEGDMA was used as a diluent. CQ (0.2 wt%), TPO (0.01 wt%), and 4-EDMAB (0.8 wt%) were added and mixed with a speed mixer (SpeedMixer DAC 150.1) at 1500 rpm for 15 min. Dental resin composites were then reinforced with NFHA at different mass ratios. The SHA-CP filled resin matrix was used as the control. Total weight of the filler amount was kept as 60 wt%. A total of 30 wt% silanized SiO_2 and 30 wt% silanized SHA-CP and NFHA fillers were premixed with the resin matrix using a speed mixer and then further blended with a three-roller mixer (EXAKT 50 EC+ Apparatebau GmbH & Co., Germany). Then, the obtained composite pastes were put into a vacuum oven at room temperature for 12 h to remove air bubbles. Afterwards, the composite paste was carefully cured using Blue-LED light (Elipar S10, 3M ESPE) using appropriate molds for the further testing.

2.3 | Characterizations

2.3.1 | Morphological evaluation of the HA structures

SEM–energy dispersive x-ray analysis (EDX) and TEM analysis were employed to observe the morphology, size, and Ca/P ratio of the fillers. SHA-CP and NHA powders were coated with Au-Pb (coating, Quorum SC7620 Mini Sputter Coater/G low Discharge System) and morphological analysis was performed with a scanning electron microscope (SEM EDX, Zeiss Sigma 300). EDX analysis of each group were performed at high magnification (×80.000) and resolution (512 by 340). EDX analysis was performed to define the mass and atomic percentage ratios (Ca/P) of the synthesized HA particles. Submicron and nanoscale structures of the synthesized CHA and NHA powders were investigated by (TEM) at 120 kV and high magnifications (×10.000–60.000).

2.3.2 | X-Ray diffraction analysis

Chemical phase analyses were conducted using the x-Ray Diffraction (XRD; PANalytical Empyrean) technique with Ni-filtered Cu-Kα radiation ($\lambda = 0.154$ nm) in the 2θ range of 10–90°, employing a scanning speed of 2° per minute at a voltage of 40 kV and a current of 200 mA. The mean crystallite sizes (D) of the powders were determined from the x-Ray Diffraction data using the Scherrer Formula70, as defined in Equation (1). In this formula, K represents Scherrer's constant, which is taken as 0.9, λ denotes the wavelength of CuKα, B corresponds to the full width at half maximum (FWHM), and θ signifies the diffraction angle.

$$D = K \times \lambda / (B \times \cos \Theta). \quad (1)$$

2.3.3 | Determination of flexural strength and flexural modulus

Flexural strength (FS) and flexural modulus (FM) of the composites were measured using a universal mechanical testing machine (AGX-V, SCHIMADZU) according to ISO 4049.[70] Five rectangular shaped specimens (25 mm × 2 mm × 2 mm, $n = 5$) of each composite paste

were prepared for the three-point bending test (span 20 mm, crosshead speed 0.75 mm/min). FS and FM were calculated in MPa with the equations given below:

$$\mathrm{FS} = 3FL/\left(2bh^2\right)\ (\mathrm{MPa}), \tag{2}$$

$$\mathrm{FM} = F\left(L^3/\left[4bdh^3\right]\right)\ (\mathrm{MPa}), \tag{3}$$

where F is the maximum load in N, L is the distance between the supports in mm, b and h are width and height, d is deflection of specimen, respectively, in mm.

2.3.4 | Determination of compressive strength

To calculate the CS of the samples, cylindrical samples with a diameter of 4 mm and a height of 6 mm were cured in a teflon mold ($n = 5$). The maximum vertical force (0.75 mm/min) at which fracture occurred was determined for the samples. The following equation was used in the calculation of the CS:

$$\mathrm{CS} = 4F/A\ (\mathrm{MPa}), \tag{4}$$

where F is maximum load in N, A is cross-sectional area of sample in millimeter s.

Vickers microhardness (VH) was determined on 3 disk-shaped specimens (Φ6 mm × 4 mm, $n = 3$) under a load of 100 g for 10 s using a micro hardness tester (HVS 1000 Microhardness Tester, Bulut Makine, Turkey). Three indents were taken for each sample. Two different measurement techniques were used for HV. For the first one composite materials were cured both of the top and bottom surfaces (VH_DC_Top). For the second evaluation, composites were cured from top of the materials and VH values were measured from top (VH_SC_Top) and bottom (VH_SC_Bottom) surfaces of the material to stimulate the clinical use. VH values were determined by the following equation by measuring the diagonal dimensions of the three indents:

$$\mathrm{VH} = 1.854F/d^2\ \left(\mathrm{kg/mm^2}\right), \tag{5}$$

where F is load in kg, d is the average length of the diagonals in mm.

2.3.5 | Determination the depth of cure

Depth of cure (DOC) was determined by preparing samples with a diameter of 4 mm and a height of 6 mm. The samples were cured from the top surface for 20 s according to ISO 4049.[70] After curing, the uncured materials on the lower surface of the samples were immediately scraped with a plastic spatula and calculated by dividing the remaining height by two. Three measurements were taken for each sample ($n = 3$).

2.3.6 | Determination the polymerization shrinkage

Polymerization shrinkage (PS) test was calculated using the Archimedes apparatus of precision balance in accordance with ISO 17304 standard.[71] Mass measurements of composite samples in dough and cured form are performed in flotation medium (sodium laurylsulphate). The shrinkage in the volumes of the samples (n = 3), whose densities were calculated from the mass and volume values, after polymerization was calculated with the following equation. Where PS is polymerization shrinkage in percent, ρ_c average of density of cured samples, ρ_u average of density of uncured samples.

$$\mathrm{PS} = \left(\left(\rho_c - \rho_u\right)/\rho_c\right) \times 100. \tag{6}$$

2.3.7 | Surface roughness and microscopic evaluation

Surface roughness and microscopic examination analyzes were performed with confocal microscope (ZEISS Smartproof 5) and optical microscope (ZEISS Smartzoom), respectively. The samples ($n = 3$) were prepared with a teflon mold of 2 mm height and 15 mm diameter. Samples cured on both sides for 20 s with a Blue-LED light source (Elipar S10, 3M ESPE) were treated with P180, P320, P600, and P800 grit sandpapers, respectively, and rinsed between each step. For polishing, the samples were polished with a broadcloth using a diamond paste solution. The samples were stored in distilled water for 7 days.

2.4 | Statistical analysis

Statistical evaluations were conducted with one-way analysis of variance (ANOVA) using SPSS software (version 17, Chicago, IL). The statistical study was carried out with ANOVA and the Tukey test. As a result of the multiple comparison method, it was accepted that there was a significant difference in the groups with a value of ($p \leq 0.05$).

3 | RESULTS AND DISCUSSION

3.1 | Morphological and chemical alteration of HA structures

The effect of the synthesis method of the HA structures on the morphology was investigated in this study. Figure 1 presents the typical SEM images of experimental groups prepared using various methods: CP, MW, HT, and SS. From the SEM images of SHA-CP (Figure 1a), it is evident that the precipitate structure is characterized by small, immature sphere-like particles that display a uniform appearance. These particles are organized into agglomerates. Such a morphology is consistent with other literature findings, suggesting this might be due to the lower sintering temperatures.[72–75] NFHA-MW and NFHA-HT particles both exhibited a good uniformity in size. In contrast, the NFHA-SS filler displayed a less uniform morphology and size, with diameters ranging between 0.8–1 μm. Nonetheless, all obtained NFHA structures displayed a globular appearance. Notably, irregular aggregations with several nanorod-shaped protrusions were observed in NFHA-MW and NFHA-SS samples. However, NFHA-HT displayed a distinctive homogeneous nanoflower-like morphology. This consists of cone-shaped nanorods that extend radially from the center, spreading out in three dimensions. The unique globular structure observed in all NFHA samples allows for concentrated stress to be channeled into the globular phases. This, in turn, facilitates stress distribution in the polymer matrix, as noted by other studies.[76,77] Such a distribution potentially prevents cracks and damage to the composites when subjected to external force, consequently enhancing the mechanical properties of the composites.[78] Based on the SEM analyses, it was determined that the HT synthesis method provided the most morphologically suitable grain structure and distribution for the target structure, when compared to the methods of CP, MW, and SS. Additionally, EDX results were showed that HA synthesis was achieved with a Ca/P ratio of approximately 1.67 in all experimental groups as it was stated in Table 1.

The TEM images are presented in Figure 2. TEM analyses were conducted to determine the grain size and distribution of samples from different groups. From the scans of thinned dark regions, we determined that the MW irradiation produced spherical nanoparticles that are homogeneously distributed. Conversely, in the SS method, the particles appeared to be stacked atop each other and exhibited relatively larger grain sizes. TEM images of the NFHA fillers synthesized using the HT revealed that rods extended radially from the center, behaving as if they were a singular particle comprised of many rods. Due to this distinctive spatial structure, concentrated stress at the tip of each rod can be transmitted to neighboring rods, resulting in a more even stress distribution within the polymer matrix. Such a distribution could prevent cracks and damage in the composites when subjected to external forces, thereby enhancing the composites' mechanical properties.

XRD analysis was used to characterize the crystal structure of the synthesized powders. XRD patterns of SHA and NFHA powders are shown in Figure 3. The diffraction peaks in Figure 3 were compared with the standard data of HA phase (ICDD 09–432, which is the standard XRD pattern of HA, and ICDD is International Centre for Diffraction Data). All the diffraction peaks in the pattern are found to be consistent with standard HA phase. It has been determined that it belongs to the hexagonal crystal system, the space group is P-6, and the space group number is 174. The lattice parameters were determined as $a = b = 9.4320$ Å and $c = 6.8810$ Å. According to XRD it has been proven that $2\theta = 10.8°$, 21.7°, 25.8°, 28.8°, 31.7°, 32.1°, 32.8°, 34.0°, 39.7°, 46.6°, 48.0°, 49.4°, 50.4°, and 53.2° peaks are to belong to the (100), (200), (002), (210), (211), (112), (300), (202), (130), (222), (132), (213), (321), and (004) planes, respectively. Furthermore, mean crystalline sizes (D) were calculated in accordance with Equation (1) and, are shown in Table 2. The crystallite size of the powders were found to be similar in all powders. Additionally, the sharp and narrow diffraction peaks are examined, which imply that SHA and NFHA powders have a highly crystalline structures. Among them, NFHA-SS was demonstrated highest crystallinity and probably this was one of the reasons of poor mechanical properties of NFHA-SS composites in this study.

3.2 | Mechanical and physical properties of dental resin composites

The robust mechanical properties of the resin composite are crucial for the long-term clinical application of dental restoratives. It is known that aggregation of spherical nanoparticles cannot be avoided completely as they are blended into organic matrixes, therefore, using different morphological structures such as nanoflower (NF) would be helpful to overcome such limitations. Herein, the reinforcing effect of SHA and NFHA on FS (FS), FM, CS (CS) and VH of the dental resins were measured. Additionally, surface roughness properties (SR), DOC, and PS behavior of the composites were determined. As shown in Table 3 and Figure 4, SHA-CP loaded samples were displayed lower FS, FM, and CS compared to NFHA

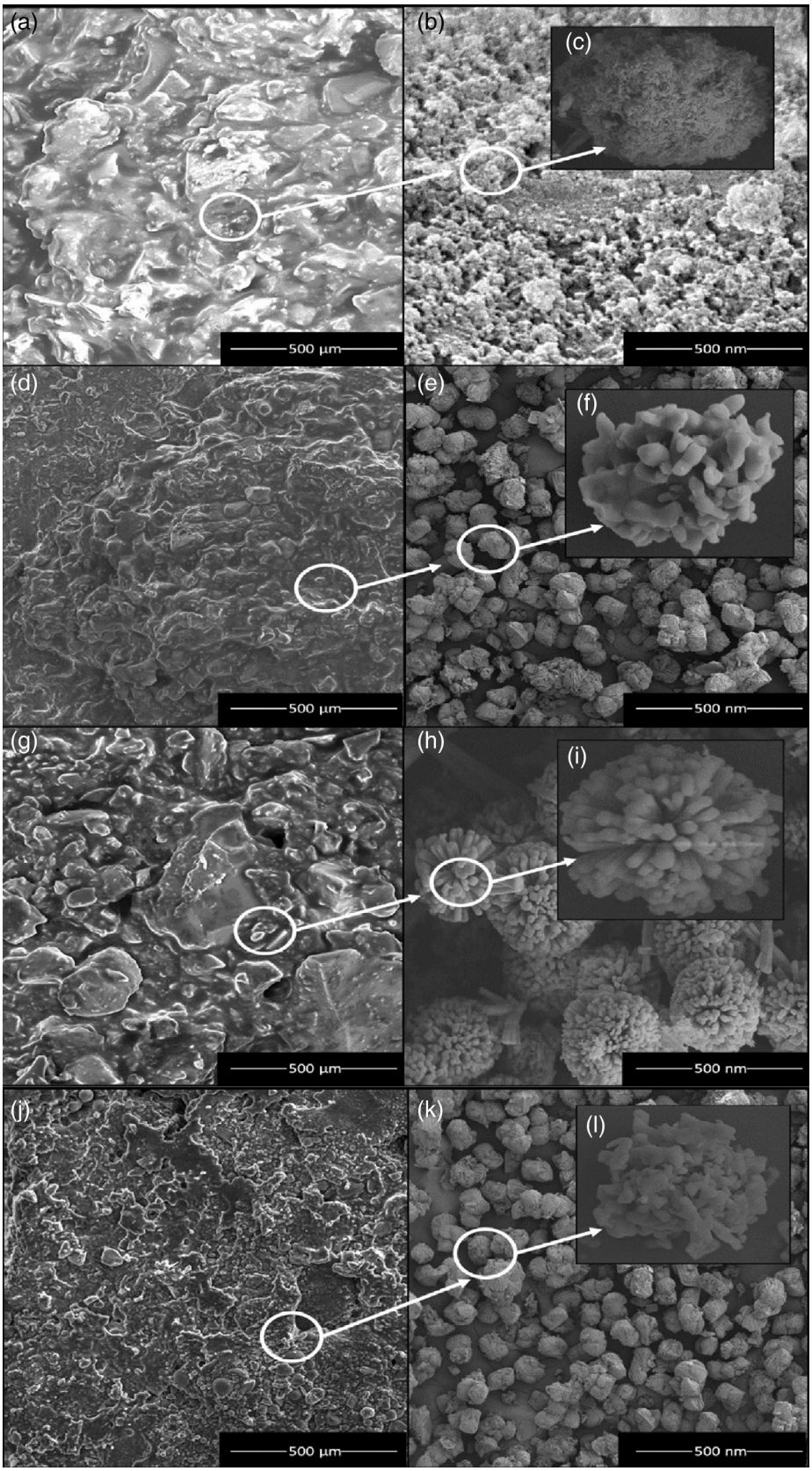

FIGURE 1 Scanning electron microscope images of hydroxyapatite particles synthesized by CP, MW, HT and SS; (a–c) SHA-CP, (d–f) NFHA-MW, (g–i) NFHA-HT, (j–l) NFHA-SS. CP, chemical precipitation; HT, hydrothermal treatment; MW, microwave irradiation; NFHA, nanoflower-like hydroxyapatite; SS, sonochemical synthesis; SHA, spherical shaped HA.

loaded samples ($p < 0.05$). With the addition of NFHA structures, the FS, FM, and CS increased in all cases ($p < 0.05$).

When the FSs of NFHA-loaded composites were compared, no significant difference was observed between the FS of NFHA-MW and NFHA-HT composites

TABLE 1 Ca/P ratio of SHA-CP, NFHA-MW, NFHA-HT, and NFHA-SS samples.

Groups	Ca (atomic %)	P (atomic %)	Ca/P
SHA-CP	62.396	37.604	1.66
NFHA-MW	62.547	37.453	1.67
NFHA-HT	62.412	37.588	1.66
NFHA-SS	62.446	37.544	1.66

Abbreviations: CP, chemical precipitation; HT, hydrothermal treatment; MW, microwave irradiation; NFHA, nanoflower-like hydroxyapatite; SS, sonochemical synthesis; SHA, spherical shaped HA.

($p = 0.108$). Similarly, there is no statistically significant difference between NFHA-HT and NFHA-SS composites in terms of FS ($p = 0.228$). However, the FS values of NFHA-MW composites are significantly higher than those of NFHA-SS composites when compared ($p = 0.002$). According to ISO 4049, the FS of the composites should be 80 MPa for Type I composites and 50 MPa for Type II composites.[70] In this context, only NFHA structures synthesized using the microwave irradiation have met the expected FS values for Type I composites. On the other hand, for Type II composites, the FS

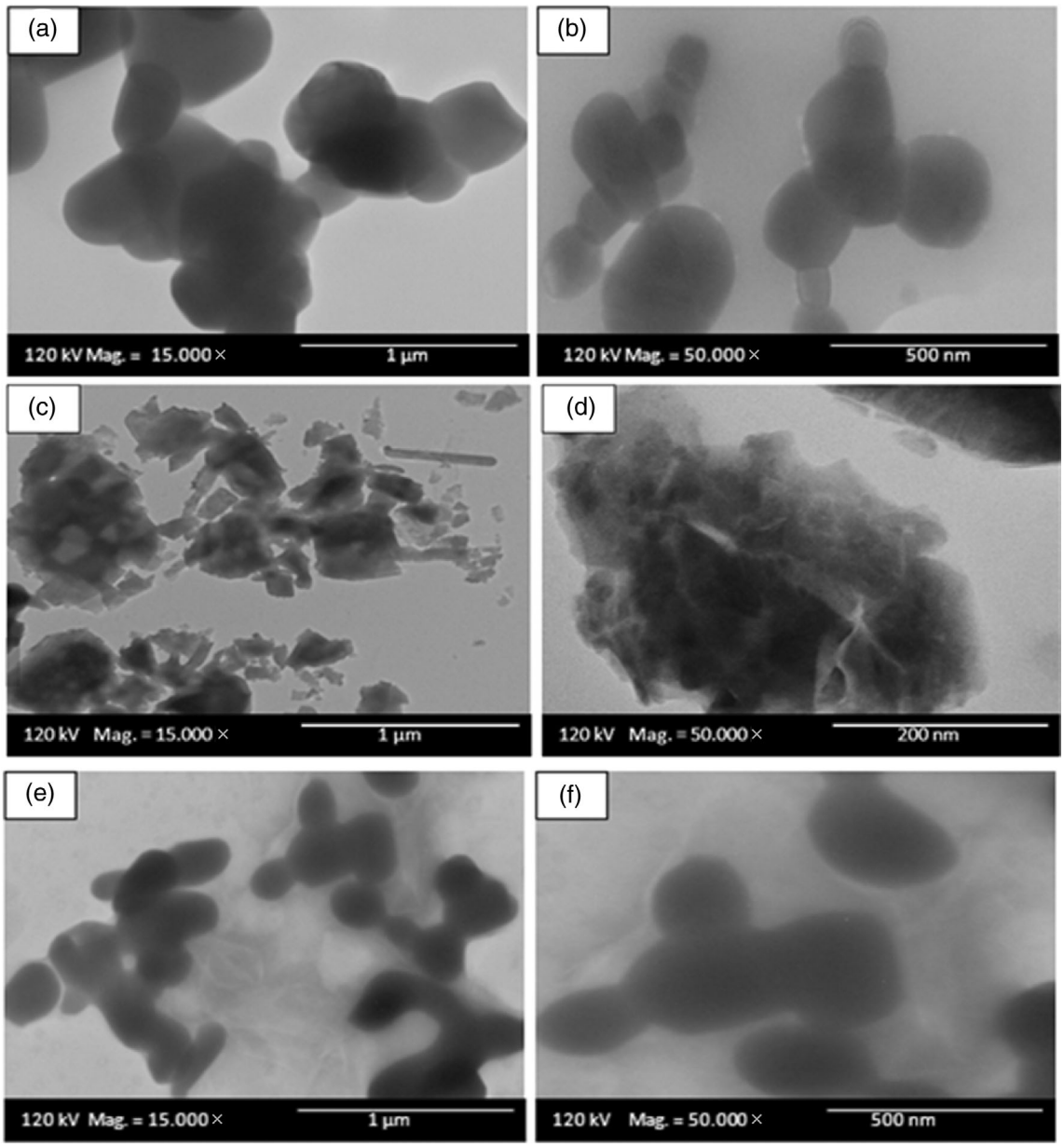

FIGURE 2 TEM images of NHA particles synthesized by CP, MW, HT, and SS (a, b) SHA-CP, (c, d) NFHA-MW, (e, f) NFHA-HT (g, h) NFHA-SS. CP, chemical precipitation; HT, hydrothermal treatment; MW, microwave irradiation; NHA, SS, sonochemical synthesis; SHA, spherical shaped HA.

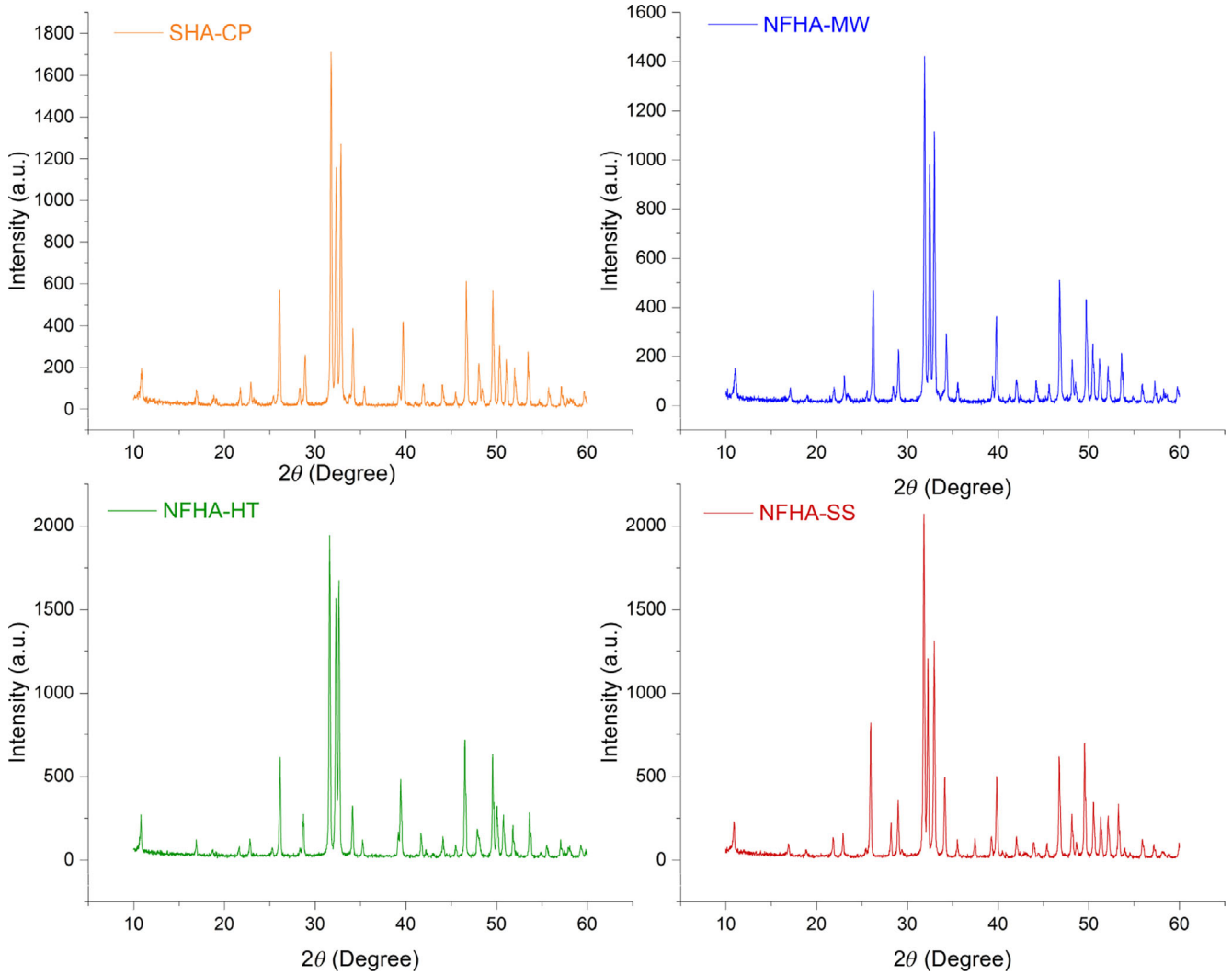

FIGURE 3 X-ray diffraction patterns of SHA-CP, NFHA-MW, NFHA-HT, and NFHA-SS. CP, chemical precipitation; HT, hydrothermal treatment; MW, microwave irradiation; NFHA, nanoflower-like hydroxyapatite; SS, sonochemical synthesis; SHA, spherical shaped HA. [Color figure can be viewed at wileyonlinelibrary.com]

TABLE 2 Mean crystallite sizes (*D*) and crystallinity values of synthesized powders.

Groups	*D* (nm)	Crystallinity (%)
SHA-CP	47.60	79
NFHA-MW	48.90	83
NFHA-HT	53.46	76
NFHA-SS	54.20	93

Abbreviations: CP, chemical precipitation; HT, hydrothermal treatment; MW, microwave irradiation; NFHA, nanoflower-like hydroxyapatite; SS, sonochemical synthesis; SHA, spherical shaped HA.

values of all composites were sufficient, but still NFHA have shown superior FS values compared to HA structures with spherical morphology as in SHA-CP.

The results were also compared with other studies in Table 4. In a study conducted by Domingo et al.,[79] all irregular-shaped nano and micro HA loaded composite structures had FS values below 56 MPa. Furthermore, composite samples obtained with HA loading without the addition of any bonding agent had FSs below 50 MPa in their study. Similarly, Calabrese et al.[80] was used HA-whiskers in their study and they reached 55 MPa maximum FS for the composites that was loaded 20 wt% HA-whiskers. Additionally, Liu et al.[81] demonstrated in a mixed silanized HAP/SiO_2 filler within a Bis-GMA/TEGDMA resin that mechanical properties such as elastic modulus, FS, and CS gradually decreased with an increase in HAP filler content. Therefore, reducing the amount of NFHA in the composites could potentially enhance the mechanical properties of the materials in this study.

In another study conducted by Chen et al.,[82] it was found that the values of biaxial flexural strength

TABLE 3 Mean ± SD values of control and experimental composite groups obtained from the 3-point bending test, compression strength test, depth of cure, polymerization shrinkage, and Vickers microhardness (VH) tests.

	SHA-CP	NFHA-MW	NFHA-HT	NFHA-SS	p[a]
Flexural strength (MPa)	56.0 ± 0.22	81.0 ± 0.25	74.0 ± 0.36	68.2 ± 0.28	0.000
Flexural modulus (GPa)	8.83 ± 0.28	7.02 ± 0.70	8.54 ± 0.60	9.58 ± 0.59	0.000
Compressive strength (MPa)	442.3 ± 4.9	556.8 ± 25.1	491.9 ± 15.2	540.2 ± 18.7	0.000
VH_DC_Top[b]	42.4 ± 1.3	42.7 ± 1.4	42.6 ± 1.28	41.2 ± 1.5	0.000
VH_SC_Top[c]	27.5 ± 2.01	27.7 ± 2.06	27.6 ± 2.04	25.5 ± 2.02	0.007
VH_SC_Bottom[d]	14.4 ± 1.01	17.9 ± 1.02	17.8 ± 1.63	15.1 ± 1.21	0.000
Depth of cure (mm)	2.87 ± 0.02	2.70 ± 0.01	2.87 ± 0.02	2.72 ± 0.03	0.000
Polymerization shrinkage (%)	2.80 ± 0.04	2.64 ± 0.08	2.68 ± 0.03	2.78 ± 0.05	0.000

Abbreviations: CP, chemical precipitation; HT, hydrothermal treatment; MW, microwave irradiation; NFHA, nanoflower-like hydroxyapatite; SS, sonochemical synthesis; SHA, spherical shaped HA.

[a]According to ANOVA.

[b]Composites were cured both on top and bottom surfaces and VH values were measured from top surface.

[c]Composites were cured on top surface, and VH values were measured from top surface.

[d]Composites were cured on top surface, and VH values were measured from bottom surface.

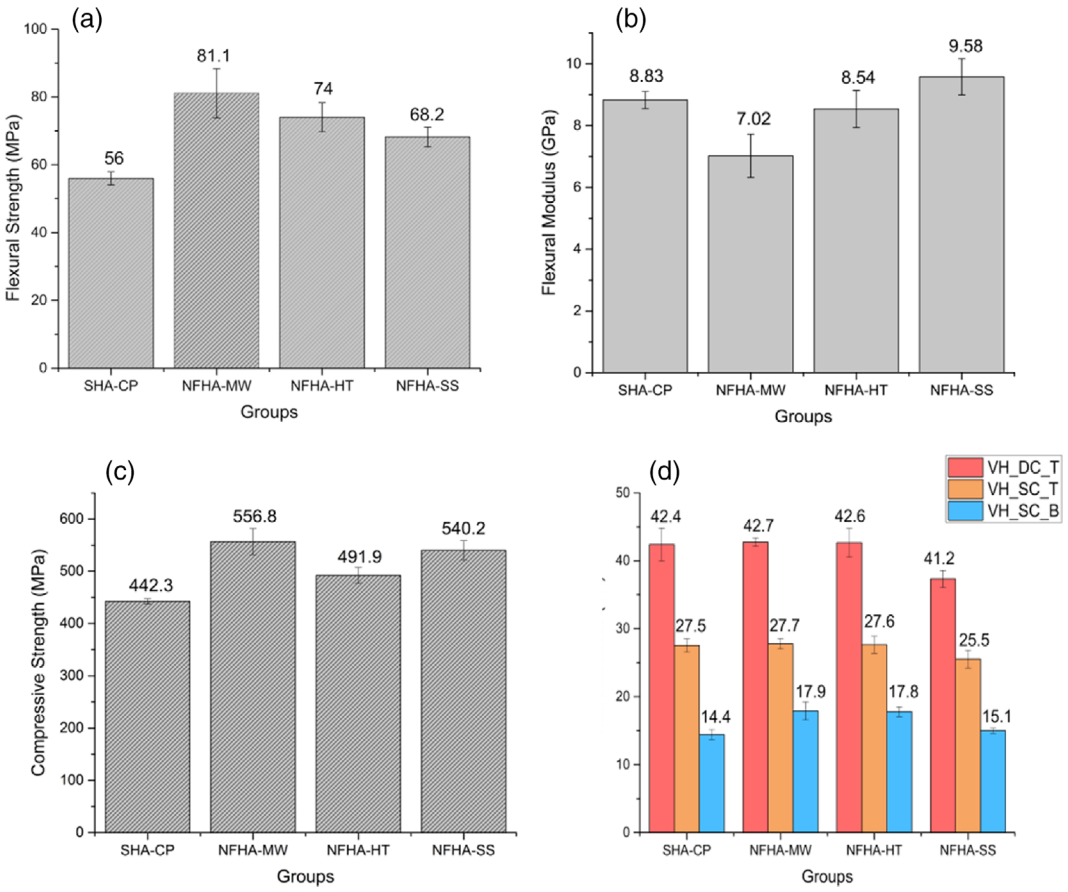

FIGURE 4 Mechanical properties of resin composites: (a) flexural strength, (b) flexural modulus, (c) compressive strength, and (d) Vickers microhardness (VH). Vertical bars indicate standard deviation. [Color figure can be viewed at wileyonlinelibrary.com]

significantly decreased for dental resins filled with 20 wt % HAP nanofibers (80.4 ± 5.7 MPa) and 40 wt% HAP nanofibers (41.7 ± 10.4 MPa) compared to the nonloaded resin formulations ($p < 0.05$). The resulted lower mechanical strength of the HA-loaded composites is not a surprise considering the nature of nano-HAP particles,

TABLE 4 Comparison of the effects of different hydroxyapatite nanoparticles on the properties of experimental dental composites.

	HA ratio (%wt)	FS (MPa)	FM (GPa)	CS (MPa)	VH	DOC (mm)	PS (%)
SHA-CP	40	56.0	8.83	442.3	42.4	2.87	2.80
NFHA-MW	40	81.0	7.02	556.8	42.7	2.70	2.64
NFHA-HT	40	74.0	8.54	491.9	42.6	2.87	2.68
NFHA-SS	40	68.2	9.58	540.2	41.2	2.72	2.78
Irregular shaped nano HA[79]	50	17.0	2.80	-	41.0	-	-
Irregular shaped micro HA[79]	60	56.0	6.20	-	46.0	-	-
HA Whisker[80]	40	55.0	3.50	-	69.0	-	-
Nano HA/silan[81]	50	≈100	≈8.50	≈250	-	≈2.5	≈3.00
HA nanofiber.[82]	60	41.7	-	-	-	-	-
HA Whisker[36]	20	≈100	≈7.00	-			
HA Particles[36]	30	≈30	≈4.00	-	≈55.0	-	-
Urchin-like HA[84]	30	≈120	4.90	≈360	80.1	-	-

Abbreviations: CP, chemical precipitation; CS, compressive strength; DOC, depth of cure; FM, flexural modulus; FS, flexural strength; HA, hydroxyapatite; HT, hydrothermal treatment; MW, microwave irradiation; NFHA, nanoflower-like hydroxyapatite; PS, polymerization shrinkage; SS, sonochemical synthesis; SHA, spherical shaped HA; VH, Vickers microhardness.

which has lower mechanical strength than SiO_2.[83] Conversely Zhang et al.[36] demonstrated that HA-whiskers does not reduce the FS of the composites at the 5–20 wt% loading rates.[36] In a recent study with similarities to ours, a novel urchin-like HA (UHA) was synthesized using MW and was utilized as a dental filler, yielding highly promising outcomes. The inclusion of UHA filler led to a notable enhancement in mechanical properties, including strength, stiffness, and microhardness. Moreover, when combined with silica nanoparticles, UHA demonstrated its optimal application by inducing a significant increase in FS, FM, and CS, with improvements of 50%, 40%, and 13%, respectively.[84] When compared to other studies in the literature, it is observed that HA structures with NF morphology enhance FS compared to spherical and irregular HA structures. Moreover, MW irradiation technique is much more efficient in terms of increasing FS, FM, and CS compared to CP, HT and SS.

The significance of the elastic modulus is primarily associated with selecting the appropriate composite material for a specific clinical scenario. The elastic modulus of resin composites depends critically on the stress transfer in the material.[85] So, presence of particles in different morphological structures would very likely lead to increase of the elastic modulus of the composites. In this study, FM values of the composites were significantly lower for NFHA-MW loaded composite materials compared to SHA-CP ($p = 0.002$), NFHA-HT ($p = 0.008$), and NFHA-SS ($p = 0.000$). Among SHA-CP, NFHA-HT, and NFHA-SS loaded composites there were no significant differences in terms of FM ($p > 0.05$). Furthermore, in accordance with other studies in the literature, the FM values obtained in the present study were found to be higher compared to most of commercial composites.[86] Taking into consideration that the primary cause of failure in posterior restorations for commercial resin composites is the brittle nature of quartz particles, the incorporation of hydroxyapatite filler in the form of whiskers, nanorods, nanofibers, and so forth, has been shown to enhance load transfer and promote toughening mechanisms. Additionally, it increases the FM and fracture toughness of unfilled resins.[87] Therefore, the use of HA structures with NF morphology in composites may offer advantages to prevent failure in the clinical usage. Compressive stress testing is employed to assess the mechanical properties of restorative materials. Given that a significant portion of masticatory forces involves compressive forces, evaluating the durability of restorative materials under such conditions holds great importance.[88] Different filler particle sizes can lead to an increased quantity of fillers within the composite matrix, thereby imparting additional strength. This relationship between an increased number of fillers and enhanced CS is well-established.[89] In this study, it was determined that the CS values of NFHA-modified composites synthesized with MW ($p = 0.000$), HT ($p = 0.001$) and SS ($p = 0.000$) increased by approximately 25%, 11%, and 22%, respectively, when compared to HA-modified composites synthesized with CP. Intergroup comparisons of NFHA-loaded resin composites revealed that there were no statistical differences between NFHA-MW and NFHA-SS ($p = 0.358$). However, CS values of these were significantly higher than NFHA-HT ($p = 0.000$ and $p = 0.001$, respectively). In comparison to other studies, the CS

values obtained in the current study were found to be higher than commercial products[90] and other HA-modified composites in the literature.[32,67,84,90–93] It is believed that the high CS values obtained in this study are due to the silanized silica structure used as the main reinforcing phase. Furthermore, since NFHA structures provide superior compressive values, it can be stated that they hold promise for increasing the longevity of restorations against chewing forces.

The incorporation of HA in restorative dentistry provides intrinsic radio-opacity, hardness closer to the ideal (similar to that of natural teeth), and consequently, improved wear resistance.[34] In this study, there was no statistically significant differences for VH values of double cured materials of NFHA-MW ($p = 0.988$) and NFHA-HT ($p = 0.995$) compared to SHA-CP on the top surface measurements. However, NFHA-SS was demonstrated the lowest VH values compared to other samples ($p < 0.05$). In addition to these results, during application, composite restorations undergo a curing process from a single surface. To simulate the application, composites were cured from a single surface, and the VH values of both the curing surfaces (VH_SC_Top) and the bottom surfaces (VH_SC_Bottom) of the structures were measured. Measurements taken from curing from a single surface yielded VH values similar to those obtained from double-sided curing. VH_SC_Top values of NFHA-MW ($p = 0.012$), NFHA-HT ($p = 0.018$), and SHA-CP ($p = 0.015$) were significantly higher compared to NFHA-SS. Furthermore, there is no significant difference among the VH_SC_Top values for NFHA-MW, NFHA-HT, and SHA-CP ($p > 0.05$). On the other hand, after curing the composites from a single surface, there have been changes in the hardness values profile at the bottom surface (VH_SC_Bottom). In this scenario, the hardness values of SHA-CP and NFHA-SS ($p = 0.722$) samples are significantly lower compared to NFHA-MW and NFHA-HT ($p = 0.998$ and $p < 0.05$). These obtained results are consistent with the curing depth results of the samples. It is believed that due to the unique morphological HA structures produced by the MW and HT methods, they can transmit more light compared to CP and SS, leading to a higher polymerization reaction and consequently higher hardness values in these structures. The utilization of VH tests is also regarded as an indirect yet accurate parameter that can be correlated with the degree of curing of resin composites, thereby reflecting the degree of conversion.[94–96] Based on the VH measurements, it can be concluded that the polymerization degrees of NFHA-MW and NFHA-HT samples are higher compared to SHA-CP and NFHA-SS. The unreacted compounds, which exhibit high mobility, have a significant impact on plastic deformation, leading to reduced strength and stiffness in the sample. In practice, if the innermost layers of composite restorations are not sufficiently cured, the elastic modulus at the base will be lower than that at the surface. This can result in increased material strain when subjected to masticatory forces.[39] Simultaneously, the nonhomogeneous crosslinking of the composite paste triggers differential PS stresses, leading to tensile stresses within the core of the resin composite. Additionally, premature failure at both low stress and strain levels could suggest a reduced cohesive strength of the dental restorative paste, potentially due to suboptimal interfacial interactions between the composite fillers and the matrix. The hardness values obtained in the current study are also found to consistent with the values of other composites modified with HA in the literature.[34,97] Furthermore NFHA structures were also demonstrated superior VH values compared to other similar studies.[67,84,98] However, it is not possible to make an assessment regarding whether these similarities with other composites are due to the morphological structure of HA or differences in the organic matrix. Briefly, the high hardness values provided by the use of HA powders produced with the MW and HT methods can offer advantages in terms of polishability, optical properties, and aesthetics.[99] Therefore, the utilization of HA powders produced through these methods in dental composites may be advantageous in practical applications.

The primary drawback of HA particles as fillers for restorative dentistry is their higher refractive index compared to the resin matrix ($n = 1.65$ vs. $n = 1.5$ for the resin).[100] Still, all DOC values obtained in the current study have met the requirement specified by ISO 4049 standard of >1.5 mm. While there is no significant difference in DOC values between SHA-CP and NFHA-SS ($p = 0.991$), as well as between NFHA-MW and NFHA-HT ($p = 0.475$), the DOC values obtained for SHA-CP and NFHA-SS are significantly lower compared to NFHA-MW and NFHA-HT ($p < 0.05$). DOC values were acceptable in this study compared to other studies that used HA as a reinforcing filler.[81] Additionally, when compared to commercial composites,[101] the DOC values of the composites modified with NFHA in the current study are in alignment with various commonly used composites.

Conventional or traditional dental composites may have PS values ranging from 2% to 5% or slightly higher.[102] Similarly, bulk-fill composites are designed for efficient and deeper restorations. They typically have slightly higher shrinkage values compared to low-shrinkage composites, often in the range of 3%–4%.[103] Some dental composite manufacturers have developed products with lower PS compared to traditional composites. These low-shrinkage composites often have

shrinkage values in the range of 1% to 2%.[103] The PS values obtained in this study fall within a range similar to that of traditional composites, approximately between 2.64% and 2.80%. The intergroup comparison was revealed that there was no significant difference found between the PS values obtained for NFHA-MW and NFHA-HT ($p = 0.125$). When comparing NFHA structures, composite samples using HA structures obtained with the SS method had the lowest PS values ($p = 0.000$). Furthermore, when compared to SHA-CP, it was determined that SHA-CP significantly reduced the PS values compared to NFHA-MW ($p = 0.000$), NFHA-HT ($p = 0.000$), and NFHA-SS ($p = 0.000$) structures. The inorganic filler typology and its percentage influence shrinkage behavior of the dental composite.[11] According to the literature findings HA loading also reduce the PS values of RBCs. The findings obtained in this study are consistent with the findings reported in the literature within the scope of the study. Experimental results obtained by Liu et al.[81] regarding the PS evolution of a resin composite at different ratios of HA/SiO_2 filler indicated that the addition of nano-HAP particles reduced the shrinkage from ~3.25% to about 2.0%. This reduction in PS was primarily attributed to the higher refractive index of HA, which influenced the crosslinking process. As the mass ratio of HA increased, a lower degree of conversion was achieved, leading to reduced shrinkage. Similarly, Al-maamori et al.[104] explained the decrease in linear shrinkage with an increasing content of micro-HA in a light-curing matrix by considering that the higher inorganic content is associated with lower polymerization values, which are directly related to shrinkage reduction. Furthermore, HA particles can act as obstacles to resin polymerization. Considering the high free energy of HA nanoparticles as filler, it can be suggested that their use allows for a higher loading ratio and thus a lower volume shrinkage in the dental composite.[105]

Surface roughness is of paramount importance in restorative dentistry as it can lead to plaque formation, discoloration, and mechanical wear of composite materials.[106] The quality of a surface can be assessed by quantifying its roughness, which highlights the fissures, streaks, or traces generated during a specific working or finishing/polishing process.[107] Ra value in surface roughness determines the vertical deviations from the initial sample. Rz refers the average roughness of the surface. Rq reflects the average quadratic deviation of the heights of the profile roughness. Hence, the surface roughness is crucial in determining the durability of the composite material. ANOVA test showed that SR values of composite was affected by the synthesis methods and different morphologies of HA structures. As seen in Table 5 SHA-CP filled materials were statistically rougher (Rz) than NFHA-MW, NFHA-HT, and NFHA-SS. Among the NFHA structures NFHA-SS filled materials showed significantly higher SR values against NFHA-MW and NFHA-HT filled composites. In terms of Rq and Rz SHA-CP composites demonstrated the highest deviations compared to NFHA-MW, NFHA-HT, and NFHA-SS. Among the NFHA structures NFHA-SS has the greater deviation compared to NFHA-MW and NFHA-HT. Compared to SHA-HS all NFHA filled materials showed significantly higher SR values. Among the NFHA structures SR values of NFHA-SS was the lowest one compared to NFHA-MW and NFHA-HT. As seen in the Figure 5, porosity attributed to the loss of particles on the surface seems to contribute less to surface roughness (Ra) in SHA-CP and NFHA-SS composite materials. On the other hand, it was greater affect on the Rz and Rq in these samples.

This present study suggested that the NFHA synthesis using microwave irradiation and hydrothermal treatment (HT) could serve as more effective reinforcing filler for dental resins/composites compared with spherical HA. NFHA synthesis using MW irradiation is superior in meeting the Type I restorative material requirements compared to other production techniques. Moreover, it is worthy of pointing out that NFHA structures was demonstrated the highest mechanical properties compared to other studies conducted with HA. Additionally, NFHA synthesis by HT and SS could be useful to meet Type II requirements in RBCs. The mechanical properties of the resulting composites could be further improved changing SiO_2, organic matrix monomers, or reducing HA amount in the composite structures. For future research, more experiments and analysis such as adjusting filler ratio and total filler loading, absorption/solubility in solvents, mechanical properties under simulated oral environment, biological

TABLE 5 Surface roughness values of working groups. (Ra: arithmetic mean of peaks and valleys, Rz: maximum roughness depth, Rq: quadratic mean of y-axis roughness values).

Surface roughness	SHA-CP	NFHA-MW	NFHA-HT	NFHA-SS
Ra (μm)	0.30	0.13	0.14	0.19
Rz (μm)	1.02	0.86	0.98	1.04
Rq (μm)	0.21	0.10	0.11	0.18

Abbreviations: CP, chemical precipitation; HT, hydrothermal treatment; MW, microwave irradiation; NFHA, nanoflower-like hydroxyapatite; SS, sonochemical synthesis; SHA, spherical shaped HA.

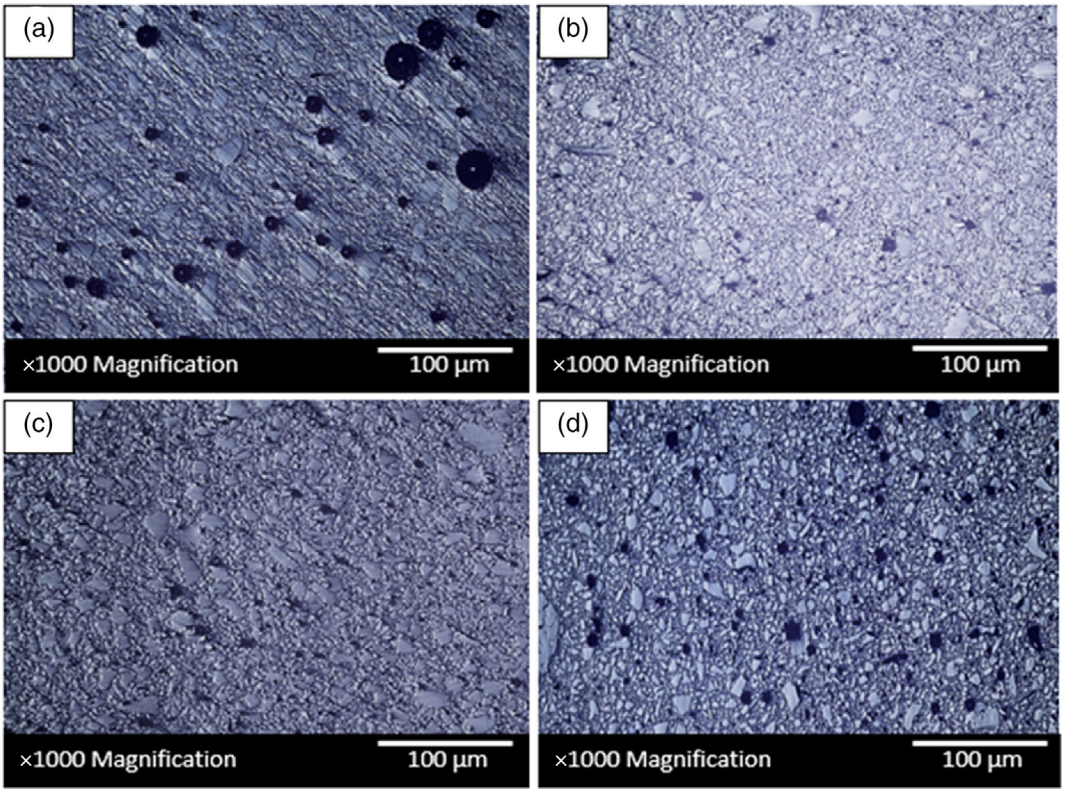

FIGURE 5 Optical microscope images working groups after surface roughness measurements at ×1.000 magnification, (a) SHA-CP, (b) NFHA-MW, (c) NFHA-HT, and (d) NFHA-SS. CP, chemical precipitation; HT, hydrothermal treatment; MW, microwave irradiation; NFHA, nanoflower-like hydroxyapatite; SS, sonochemical synthesis; SHA, spherical shaped HA. [Color figure can be viewed at wileyonlinelibrary.com]

tests, should be conducted on NFHA filled dental resin composites.

4 | CONCLUSION

In this study spherical hydroxyapatite was synthesized using CP and the nanoflower hydroxyapatite was successfully synthesized by MW, HT, and SS and resin based dental composites were fabricated. Compared with silanized SHA and other studies in the literature, silanized NFHA with unique spatial structure were increased the mechanical and physical properties of the resulting composites. Specially, NFHA-MW was leaded to a higher mechanical strength than that of the dental resins with NFHA-HT and NFHA-SS. Consequently, the innovative nanoflower-like hydroxyapatite has the potential to serve as a promising filler for producing dental resin composites with enhanced mechanical properties and potential bioactivity.

AUTHOR CONTRIBUTIONS

Kadir Sağır: Investigation (equal); methodology (equal); writing – original draft (equal). **Aysu Aydınoğlu:** Conceptualization (lead); data curation (lead); investigation (equal); methodology (lead); project administration (lead); supervision (lead); visualization (lead); writing – original draft (equal). **Afife Binnaz Hazar Yoruç:** Methodology (equal); supervision (supporting); writing – review and editing (supporting).

ACKNOWLEDGMENTS

This work has been supported by Yildiz Technical University Scientific Research Projects Coordination Unit under project number FBA-2020-3992.

CONFLICT OF INTEREST STATEMENT

The authors declare that they have no known competing financial interests or personal relationships that could have appeared to influence the work reported in this paper.

DATA AVAILABILITY STATEMENT

All data obtained within the scope of the study are provided in the article.

ORCID

Aysu Aydınoğlu https://orcid.org/0000-0002-1875-2249

REFERENCES

[1] M. Siang Soh, A. Sellinger, A. Uj Yap, *Curr. Nanosci.* **2006**, *2*, 373.
[2] E. Habib, R. Wang, Y. Wang, M. Zhu, X. X. Zhu, *ACS Biomater. Sci. Eng.* **2016**, *2*, 1.
[3] N. Moszner, U. Salz, *Macromol. Mater. Eng.* **2007**, *292*, 245.
[4] J. H. Berg, T. P. Croll, *Pediatr. Dent.* **2015**, *37*, 116.
[5] W. A. Ricci, N. Fahl Jr., *J. Esthet. Restor. Dent.* **2023**, *35*, 7.
[6] A. Vichi, A. Fraioli, C. L. Davidson, M. Ferrari, *Dent. Mater.* **2007**, *23*, 1584.
[7] C. A. Stewart, Y. Finer, *Dent. Mater.* **2019**, *35*, 36.
[8] W. Zhou, S. Liu, X. Zhou, M. Hannig, S. Rupf, J. Feng, X. Peng, L. Cheng, *Int. J. Mol. Sci.* **2019**, *20*, 723.
[9] J. L. Ferracane, W. M. Palin, *Non-Metallic Biomaterials for Tooth Repair and Replacement*, Elsevier, Philadelphia **2013**, p. 294.
[10] F. F. Demarco, M. B. Corrêa, M. S. Cenci, R. R. Moraes, N. J. M. Opdam, *Dent. Mater.* **2012**, *28*, 87.
[11] J. L. Ferracane, *Dent. Mater.* **2011**, *27*, 29.
[12] Y. Wang, M. Zhu, X. X. Zhu, *Acta Biomater.* **2021**, *122*, 50.
[13] H. H. K. Xu, *J. Dent. Res.* **1999**, *78*, 1304.
[14] L. D. Randolph, W. M. Palin, G. Leloup, J. G. Leprince, *Dent. Mater.* **2016**, *32*, 1586.
[15] M. Tian, Y. Gao, Y. Liu, Y. Liao, N. E. Hedin, H. Fong, *Dent. Mater.* **2008**, *24*, 235.
[16] F. Elfakhri, R. Alkahtani, C. Li, J. Khaliq, *Ceram. Int.* **2022**, *48*, 27280.
[17] A. Mebert, C. Baglole, M. Desimone, D. Maysinger, *Food Chem. Toxicol.* **2017**, *109*, 753.
[18] M. S. Islam, M. Nassar, M. A. Elsayed, D. B. Jameel, T. T. Ahmad, M. M. Rahman, *Polymers* **2023**, *9*, 2121.
[19] S. Imamura, H. Takahashi, I. Hayakawa, P. Loyaga-Rendon, S. Minakuchi, *Dent. Mater. J.* **2008**, *27*, 802.
[20] C. Poggio, R. Beltrami, A. Scribante, M. Colombo, M. Chiesa, *Dent. Res. J.* **2012**, *9*, 567.
[21] J.-K. Park, T.-H. Kim, C.-C. Ko, F. García-Godoy, H.-I. Kim, Y. H. Kwon, *Am. J. Dent.* **2010**, *23*, 39.
[22] S.-Y. Fu, X.-Q. Feng, B. Lauke, Y.-W. Mai, *Composites, Part B* **2008**, *39*, 933.
[23] A. Siot, C. Longuet, R. Léger, B. Otazaghine, P. Ienny, A.-S. Caro-Bretelle, N. Azéma, *Polym. Test.* **2018**, *70*, 92.
[24] J. L. Ferracane, T. J. Hilton, J. W. Stansbury, D. C. Watts, N. Silikas, N. Ilie, S. Heintze, M. Cadenaro, R. Hickel, *Dent. Mater.* **2017**, *33*, 1171.
[25] L. D. Randolph, W. M. Palin, J. G. Leprince, *Dental Composite Materials for Direct Restorations*, Sipringer, New York **2018**, p. 11.
[26] Z. Fu, Y. Zhuang, J. Cui, R. Sheng, H. Tomás, J. Rodrigues, B. Zhao, X. Wang, K. Lin, *Eng. Regen.* **2022**, *3*, 163.
[27] J. E. Frencken, M. C. Peters, D. J. Manton, S. C. Leal, V. V. Gordan, E. Eden, *Int. Dent. J.* **2012**, *62*, 223.
[28] L. I. Dakkouri, Development of novel remineralising antibacterial dental composite. **2015**.
[29] C. d. C. A. Lopes, P. H. J. O. Limirio, V. R. Novais, P. Dechichi, *Appl. Spectrosc. Rev.* **2018**, *53*, 747.
[30] J. de Dios Teruel, A. Alcolea, A. Hernández, A. J. O. Ruiz, *Arch. Oral Biol.* **2015**, *60*, 768.
[31] E. Pepla, L. K. Besharat, G. Palaia, G. Tenore, G. Migliau, *Ann. Stomatol.* **2014**, *5*, 108.
[32] F. Liu, X. Jiang, Q. Zhang, M. Zhu, *Compos. Sci. Technol.* **2014**, *101*, 86.
[33] J. Liu, H. Zhang, H. Sun, Y. Liu, W. Liu, B. Su, S. Li, *Materials* **2021**, *14*, 5612.
[34] R. W. Arcís, A. López-Macipe, M. Toledano, E. Osorio, R. Rodríguez-Clemente, J. Murtra, M. A. Fanovich, C. D. Pascual, *Dent. Mater.* **2002**, *18*, 49.
[35] N. Kantharia, S. Naik, S. Apte, M. Kheur, S. Kheur, B. Kale, *Bone* **2014**, *34*, 1.
[36] H. Zhang, B. W. Darvell, *Dent. Mater.* **2012**, *28*, 824.
[37] R. Labella, M. Braden, S. Deb, *Biomaterials* **1994**, *15*, 1197.
[38] W. D. Cook, *Aust. Dent. J.* **1981**, *26*, 105.
[39] V. C. B. Leitune, F. M. Collares, R. M. Trommer, D. G. Andrioli, C. P. Bergmann, S. M. W. Samuel, *J. Dent.* **2013**, *41*, 321.
[40] R. N. Jardim, A. A. Rocha, A. M. Rossi, A. de Almeida Neves, M. B. Portela, R. T. Lopes, T. M. Pires dos Santos, Y. Xing, E. Moreira da Silva, *J. Mech. Behav. Biomed. Mater.* **2020**, *109*, 103817.
[41] S. Utneja, S. Talwar, R. R. Nawal, S. Sapra, M. Mittal, A. Rajain, M. Verma, *J. Conserv. Dent. JCD* **2018**, *21*, 681.
[42] L. Qin, S. Yao, W. Meng, J. Zhang, R. Shi, C. Zhou, J. Wu, *Dent. Mater.* **1989**, *2022*, 38.
[43] A. Turkistani, S. Nakashima, Y. Shimada, J. Tagami, A. Sadr, *J. Dent. Res.* **2015**, *94*, 1070.
[44] W. Suchanek, M. Yoshimura, *J. Mater. Res.* **1998**, *13*, 94.
[45] S. Balhuc, R. Campian, A. Labunet, M. Negucioiu, S. Buduru, A. Kui, *Crystals* **2021**, *11*, 674.
[46] S. Zinatloo-Ajabshir, M. Emsaki, G. Hosseinzadeh, *J. Colloid Interface Sci.* **2022**, *619*, 1.
[47] K. Mahdavi, S. Zinatloo-Ajabshir, Q. A. Yousif, M. Salavati-Niasari, *Ultrason. Sonochem.* **2022**, *82*, 105892.
[48] N. Timpe, H. Fullriede, L. Borchers, M. Stiesch, P. Behrens, H. Menzel, *BioNanoMaterials* **2014**, *15*, 89.
[49] A. Aminoroaya, R. E. Neisiany, S. N. Khorasani, P. Panahi, O. Das, H. Madry, M. Cucchiarini, S. Ramakrishna, *Composites, Part B* **2021**, *216*, 108852.
[50] M. Lezaja, D. N. Veljovic, B. M. Jokic, I. Cvijovic-Alagic, M. M. Zrilic, V. Miletic, *J. Biomed. Mater. Res. Part B* **2013**, *101*, 1469.
[51] Z. Sun, Y. Jiang, Z. Cong, B. Zhao, F. Shen, X. Han, *Nanotechnology* **2021**, *32*, 285401.
[52] N. T. Kalyani, S. J. Dhoble, *Quantum Dots*, Elsevier, Kidlington **2023**, p. 3.
[53] I. R. Mary, S. Sonia, S. Viji, D. Mangalaraj, C. Viswanathan, N. Ponpandian, *Appl. Surf. Sci.* **2016**, *361*, 25.
[54] A. Lak, M. Mazloumi, M. Mohajerani, A. Kajbafvala, S. Zanganeh, H. Arami, S. K. Sadrnezhaad, *J. Am. Ceram. Soc.* **2008**, *91*, 3292.
[55] J. Liu, K. Li, H. Wang, M. Zhu, H. Yan, *Chem. Phys. Lett.* **2004**, *396*, 429.
[56] S. V. Panin, V. O. Alexenko, D. G. Buslovich, *Polymers* **2022**, *14*, 975.
[57] R. Teghil, M. Curcio, A. De Bonis, *Coatings* **2021**, *11*, 811.
[58] C. Sanchez, H. Arribart, M. M. Giraud Guille, *Nat. Mater.* **2005**, *4*, 277.
[59] S. J. Lee, H. Jang, *Nanoscale Adv.* **2023**, *5*, 5165.
[60] G. N. Kokila, C. Mallikarjunaswamy, V. L. Ranganatha, *Inorg. Nano-Met. Chem.* **2022**, *14*, 90.

[61] G. Yang, S.-J. Park, *Materials* **2019**, *12*, 1177.
[62] L.-Y. Meng, B. Wang, M.-G. Ma, K.-L. Lin, *Mater. Today Chem.* **2016**, *1–2*, 63.
[63] A. K. Shukla, Nanotechnology for Dentistry Applications, IOP Publishing, United Kingdom **2021**, p. 3.
[64] A. B. H. Yoruç, A. Aydınoğlu, *Mater. Sci. Eng. C* **2017**, *75*, 934.
[65] A. Cüneyt Tas, *Biomaterials* **2000**, *21*, 1429.
[66] J. Liu, K. Li, H. Wang, M. Zhu, H. Xu, H. Yan, *Nanotechnology* **2004**, *16*, 82.
[67] L. Qian, R. Wang, W. Li, H. Chen, X. Jiang, M. Zhu, *Macromol. Mater. Eng.* **2019**, *304*, 1800738.
[68] C. Qi, Y.-J. Zhu, C.-T. Wu, T.-W. Sun, Y.-Y. Jiang, Y.-G. Zhang, J. Wu, F. Chen, *RSC Adv.* **2016**, *6*, 9686.
[69] A. Aydınoğlu, A. B. H. Yoruç, *Mater. Sci. Eng. C* **2017**, *79*, 382.
[70] ISO 4049: 2019, Dentistry: Polymer-based restorative materials, International Organization for Standardization.
[71] ISO 17304 (2013), Dentistry - Polymerization shrinkage: Method for determination of polymerisation shrinkage of polymer-based restorative materials, International Organization for Standardization.
[72] S. K. Avinashi, P. Singh, Shweta, K. Sharma, A. Hussain, D. Singh, C. Gautam, *Ceram. Int.* **2022**, *48*, 18475.
[73] J. Latocha, M. Wojasiński, P. Sobieszuk, S. Gierlotka, T. Ciach, *Ceram. Int.* **2019**, *45*, 21220.
[74] A. Afshar, M. Ghorbani, N. Ehsani, M. R. Saeri, C. C. Sorrell, *Mater. Des.* **2003**, *24*, 197.
[75] A. Yelten-Yilmaz, S. Yilmaz, *Ceram. Int.* **2018**, *44*, 9703.
[76] Y. Wang, J. Shi, L. Han, F. Xiang, *Mater. Sci. Eng., A* **2009**, *501*, 220.
[77] J. Shi, Y. Wang, L. Liu, H. Bai, J. Wu, C. Jiang, Z. Zhou, *Mater. Sci. Eng., A* **2009**, *512*, 109.
[78] J. Zhu, H. Peng, F. Rodriguez-Macias, J. L. Margrave, V. N. Khabashesku, A. M. Imam, K. Lozano, E. V. Barrera, *Adv. Funct. Mater.* **2004**, *14*, 643.
[79] C. Domingo, R. W. Arcís, A. López-Macipe, R. Osorio, R. Rodríguez-Clemente, J. Murtra, M. A. Fanovich, M. Toledano, *J. Biomed. Mater. Res.* **2001**, *56*, 297.
[80] L. Calabrese, F. Fabiano, M. Currò, C. Borsellino, L. M. Bonaccorsi, V. Fabiano, R. Ientile, E. Proverbio, *Adv. Mater. Sci. Eng.* **2016**, *2016*, 2172365.
[81] F. W. Liu, J. H. Hu, R. L. Wang, Y. Y. Pan, X. Z. Jiang, M. F. Zhu, *Materials Science Forum*, Vol. 745, Trans Tech Publ, Taiyuan **2013**, p. 466.
[82] L. Chen, Q. Yu, Y. Wang, H. Li, *Dent. Mater.* **2011**, *27*, 1187.
[83] C. Domingo, R. W. Arcís, E. Osorio, R. Osorio, M. A. Fanovich, R. Rodríguez-Clemente, M. Toledano, *Dent. Mater.* **2003**, *19*, 478.
[84] F. Liu, B. Sun, X. Jiang, S. S. Aldeyab, Q. Zhang, M. Zhu, *Dent. Mater.* **2014**, *30*, 1358.
[85] R. W. Bryant, D. B. Mahler, *J. Prosthet. Dent.* **1986**, *56*, 243.
[86] A. Scribante, M. Bollardi, M. Chiesa, C. Poggio, M. Colombo, *Biomed Res. Int.* **2019**, *2019*, 5109481.
[87] F. Fabiano, L. Calabrese, E. Proverbio, *Materials for Biomedical Engineering*, Elsevier, Holland **2019**, p. 251.
[88] J. A. Mohandesi, M. A. Rafiee, V. Barzegaran, F. Shafiei, *Dent. Mater. J.* **2007**, *26*, 827.
[89] Y. Papadogiannis, R. S. Lakes, G. Palaghias, M. Helvatjoglu-Antoniades, D. Papadogiannis, *Dent. Mater.* **2007**, *23*, 235.
[90] Moezzyzadeh, M. **2012**.
[91] B. Pratap, R. K. Gupta, B. Bhardwaj, M. Nag, *Mater. Today Proc.* **2020**, *33*, 2567.
[92] M. Sabir, A. Ali, U. Siddiqui, N. Muhammad, A. S. Khan, F. Sharif, F. Iqbal, A. T. Shah, A. Rahim, I. U. Rehman, *J. Biomater. Sci. Polym. Ed.* **2020**, *31*, 1806.
[93] S.-N. Zhao, D.-L. Yang, D. Wang, Y. Pu, Y. Le, J.-X. Wang, J.-F. Chen, *J. Mater. Sci.* **2019**, *54*, 3878.
[94] R. H. Halvorson, R. L. Erickson, C. L. Davidson, *Dent. Mater.* **2003**, *19*, 327.
[95] J. L. Ferracane, E. H. Greener, *J. Dent. Res.* **1984**, *63*, 1093.
[96] J. G. Leprince, P. Leveque, B. Nysten, B. Gallez, J. Devaux, G. Leloup, *Dent. Mater.* **2012**, *28*, 512.
[97] D. D. da Silva Parize, J. E. de Oliveira, T. Williams, D. Wood, R. de Jesús Avena-Bustillos, A. P. Klamczynski, G. M. Glenn, J. M. Marconcini, L. H. C. Mattoso, *Carbohydr. Polym.* **2017**, *174*, 923.
[98] F. W. Liu, S. Bao, Y. Jin, X. Z. Jiang, M. F. Zhu, *Mater. Res. Innovations* **2014**, *18*, S4.
[99] N. Moszner, S. Klapdohr, *Int. J. Nanotechnol.* **2004**, *1*, 130.
[100] I. E. Ruyter, H. Øysæd, *Acta Odontol. Scand.* **1982**, *40*, 179.
[101] B. K. Moore, J. A. Platt, G. Borges, T.-M. G. Chu, I. Katsilieri, *Oper. Dent.* **2008**, *33*, 408.
[102] G. S. S. Lin, N. R. N. Abdul Ghani, N. H. Ismail, K. P. Singbal, N. M. M. Yusuff, *Eur. J. Dent.* **2020**, *14*, 448.
[103] R. J.-Y. Kim, Y.-J. Kim, N.-S. Choi, I.-B. Lee, *J. Dent.* **2015**, *43*, 430.
[104] M. H. Al-Maamori, S. H. Awad, A. K. Hussein, *Int. J. Curr. Eng. Technol.* **2014**, *4*, 2151.
[105] B. S. Oduncu, S. Yucel, I. Aydin, I. D. Sener, G. Yamaner, *World Acad Sci Eng Technol* **2010**, *40*, 286.
[106] T. Imtiaz, S. B. Ganesh, S. Jayalakshmi, *J. Adv. Pharm. Technol. Res.* **2022**, *13*, S466.
[107] A. D. Popescu, M. J. Tuculina, O. A. Diaconu, L. M. Gheorghiță, C. Nicolicescu, C. N. Cumpătă, C. Petcu, J. Abdul-Razzak, A. M. Rîcă, R. Voinea-Georgescu, *Medicina* **2023**, *59*, 59.

How to cite this article: K. Sağır, A. Aydınoğlu, A. B. Hazar Yoruç, *J. Appl. Polym. Sci.* **2024**, e55347. https://doi.org/10.1002/app.55347